REVIEW

doi:10.1038/nature11032

Deformation cycles of subduction earthquakes in a viscoelastic Earth

Kelin Wang[1,2], Yan Hu[2]† & Jiangheng He[1]

Subduction zones produce the largest earthquakes. Over the past two decades, space geodesy has revolutionized our view of crustal deformation between consecutive earthquakes. The short time span of modern measurements necessitates comparative studies of subduction zones that are at different stages of the deformation cycle. Piecing together geodetic 'snapshots' from different subduction zones leads to a unifying picture in which the deformation is controlled by both the short-term (years) and long-term (decades and centuries) viscous behaviour of the mantle. Traditional views based on elastic models, such as coseismic deformation being a mirror image of interseismic deformation, are being thoroughly revised.

A subduction fault may stay 'locked' for centuries and then suddenly slip to cause an earthquake. Coseismic slip of tens of metres can cause devastating shaking and tsunami, as most recently demonstrated by the moment magnitude (M_w) = 9 Tohoku, Japan, earthquake of 11 March 2011. The rupture and the subsequent evolution of stress and strain leading to the next earthquake is loosely called a subduction earthquake cycle (SEC). When the theory of plate tectonics had just gained wide acceptance, the role of mantle creep in SEC was postulated[1,2] to reconcile the overall steady motion of tectonic plates and the jerky deformation at their boundaries due to great earthquakes. In this early model, SEC stress fluctuations propagate as one-dimensional diffusion waves through an elastic plate overlying a viscous asthenosphere (Fig. 1a). Its prediction that the strongest elastic deformation should be found near plate boundaries proved correct and provided guidance for geodetic studies of SEC in the ensuing decades. Maxwell viscoelasticity was first applied to earthquake models in the 1970s (ref. 3), in recognition that the deep Earth can elastically transmit stress yet behaves like a viscous fluid that hosts mantle convection and causes delayed response to the removal of surface ice load (see review in ref. 4). Two-dimensional modelling efforts (Fig. 1b) in the 1980s (see review in ref. 5), especially those to explain century-long deformation records of the Nankai subduction zone, southwest Japan[6,7], established that three primary processes took place after each great earthquake (Fig. 2). These are: (1) continuing slip of the fault (now called 'afterslip'), most evidently downdip of the rupture zone, (2) viscoelastic relaxation of the earthquake-induced stress, and (3) relocking of the subduction fault. These modelling efforts also led to the view that asthenosphere viscosity at subduction zones is about 10^{19} Pa s, one to two orders of magnitude lower than the global average[8]. However, the two-dimensional perspective failed to account for the fact that the duration of postseismic relaxation scales with rupture length in the third dimension. The consequent lack of universal success raised doubts about the importance of viscous deformation in SEC[9].

The launch of the Global Positioning System (GPS) revolutionized crustal deformation measurements. Since the early 1990s, GPS measurements, either in campaign style or as continuous monitoring, have delineated patterns of co-, post- and interseismic deformation for many

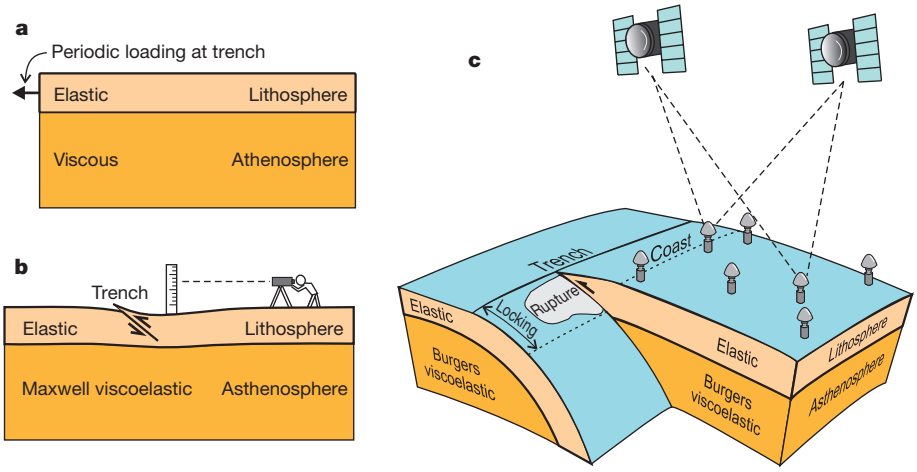

Figure 1 | Representative SEC models and development of observation technology. **a**, One-dimensional stress diffusion model of 1973 (ref. 2) based on ref. 1, a predictive model guiding future observations. **b**, Two-dimensional Maxwell viscoelastic model of 1984 (ref. 6). Observations were based mainly on terrestrial geodesy, especially repeat levelling surveys. **c**, Three-dimensional Burgers viscoelastic model, used in this review. Today, space geodesy, especially GPS (satellites and antennas shown), is the most common means of observing contemporary crustal deformation.

[1]Pacific Geoscience Centre, Natural Resources Canada, Geological Survey of Canada, Sidney, British Columbia V8L 4B2, Canada. [2]School of Earth and Ocean Sciences, University of Victoria, Victoria, British Columbia V8W 3V6, Canada. †Present address: Geophysical Institute, University of Alaska, Fairbanks, Alaska 99775, USA.

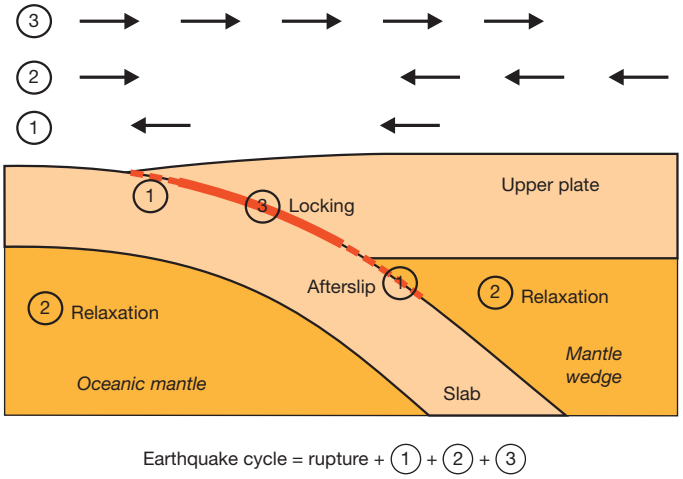

Figure 2 | Three primary processes after a subduction earthquake. (1) Aseismic afterslip occurs mostly around the rupture zone, (2) the coseismically stressed mantle undergoes viscoelastic relaxation, and (3) the fault is relocked. Arrows at the top show the sense of horizontal motion of Earth's surface, relative to distant parts of the upper plate, caused by each of these three processes.

subduction zones with unprecedented clarity. Developments in satellite radar interferometry and satellite gravimetry further improved the situation. In the meantime, progress in computing technology has enabled numerical viscoelastic SEC models that more accurately represent three-dimensional Earth structure and rupture geometry[10–14] (Fig. 1c). However, the vast majority of the SEC models developed in this new era, especially those focused on fault locking or fault friction, assume a purely elastic Earth.

High-quality modern geodetic observations have been widely available for only one to two decades. For each subduction zone, they provide merely a 'snapshot' of its SEC evolution. The main reason for the popularity of the elastic model is the convenience it offers in inferring the apparent state of fault locking from each snapshot. However, it has become evident that these snapshots collectively reflect a common deformation cycle that includes the above-mentioned three primary processes (Fig. 2). Since the 1980s, the most important progress includes the stronger evidence for very low viscosities of the mantle wedge, the recognition that postseismic viscoelastic relaxation consists of both transient and steady-state phases, as well as much improved knowledge of afterslip. In this review, we also emphasize that the characteristic time of the relaxation depends strongly on earthquake size.

Observing subduction earthquake cycles

When GPS first became available, it only confirmed what had already been inferred from sparse terrestrial geodetic measurements that many subduction faults are currently locked and accumulating strain energy for future earthquakes. An example is the Cascadia subduction zone[15,16], where an $M_w \approx 9$ subduction earthquake occurred in 1700, and GPS sites are now moving landward with respect to the remote areas of the upper plate (Fig. 3c). Soon, intriguing GPS velocities were reported from Chile[17,18] and Alaska[19] where a $M_w = 9.5$ and a $M_w = 9.2$ earthquake occurred in 1960 and 1964, respectively. These data show coastal sites to be moving landward as seen at other locked subduction zones, but inland sites some 200–400 km from the trench to be moving seaward (Fig. 3b). In 2004, a devastating $M_w = 9.2$ earthquake ruptured the Sumatra margin. Most strikingly, GPS sites in a very large area of the upper plate have been moving seaward ever since, in the same direction as their coseismic motion[20–22] (Fig. 3a). In March 2011, the $M_w = 9$ Tohoku earthquake and its tsunami devastated northeastern Japan. Similarly to Sumatra, terrestrial GPS sites in northeastern Japan have been moving seaward since the earthquake (http://www.gsi.go.jp/chibankansi/chikakukansi40005.html; in Japanese).

A pattern of SEC evolution for giant earthquakes thus emerged. It features a progressive reversal of motion direction away from the rupture zone: wholesale seaward motion, followed by opposing motion of the coastal and inland areas, and eventual wholesale landward motion. This evolution, in a more convincing way than did the Nankai levelling data[6], invalidates a popular belief that interseismic deformation is a subdued mirror image of coseismic deformation. In retrospect, we can see that the one-dimensional stress-diffusion model (Fig. 1a) four decades ago[1,2] would have predicted the opposing motion currently seen at Chile and Alaska, but it took space geodesy to rediscover it.

Viscoelastic mantle relaxation

In laboratory experiments, rock creep exhibits an initial transient phase of rapid change and a subsequent steady-state phase[23] (see Box 1). Traditionally, the study of rock creep is focused on the steady-state

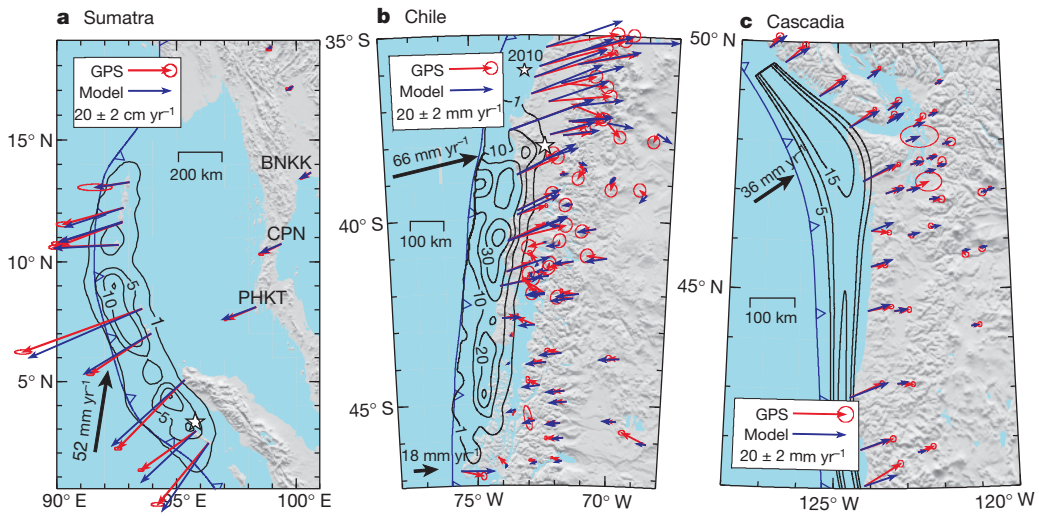

Figure 3 | GPS- (red) and model-predicted (blue) surface velocities for three subduction zones that are at different stages of the earthquake cycle. a, At Sumatra, one year after the $M_w = 9.2$ earthquake of 2004 (refs 20 and 21) (epicentre shown by star), all sites move seaward. Shown are ~1-year average GPS velocities. More recent data show the same pattern[22]. Coseismic fault slip (contoured in metres) is based on ref. 56. Longer (~3-years) time series from the three labelled far-field sites (BNKK, CPN, PHKT)[32] helped constrain afterslip and transient rheology (ref. 48). **b**, At Chile, four decades after the $M_w = 9.5$ earthquake of 1960, coastal and inland sites show opposing motion. Coseismic slip is from ref. 14. For sources of GPS data, see ref. 17. The northernmost areas show wholesale landward motion before the 2010 $M_w = 8.8$ Maule earthquake. **c**, At Cascadia, three centuries after the $M_w \approx 9$ earthquake of 1700, all sites move landward. The model is an updated version of ref. 8. A more comprehensive GPS compilation shows a similar deformation pattern[16].

BOX 1
Steady-state and transient rheology

Under temperature (T) and pressure (P) conditions appropriate for the lower crust and mantle, if a rock specimen is loaded with a constant stress σ, it undergoes an initial elastic deformation $\dot{\varepsilon}_E$, then transient creep of rapidly changing strain rate $\dot{\varepsilon}_T$, and eventually steady-state creep of constant strain rate $\dot{\varepsilon}_S$ (see Box 1 Fig. 1). Different loading stresses result in different steady-state strain rates. These pairs of σ and $\dot{\varepsilon}_S$ define the commonly seen steady-state flow law[57] $\dot{\varepsilon}_S = D\sigma^n \exp[-(Q+PV)/RT]$, where the parameter D depends on the rock composition, grain size, and fluid content, and n, Q, V and R are all constants.

The value of the stress exponent n depends on the microscopic deformation mechanism[28,57]. For example, creep due to mass diffusion leads to $n = 1$, but creep due to migration of dislocations in crystalline lattice structure leads to $n \approx 3$. If transient creep is ignored, the viscoelastic rock deformation can be described using the Newtonian ($n = 1$) or non-Newtonian ($n > 1$) Maxwell fluid, which can be envisioned as an elastic element with shear modulus (rigidity) μ_M and bulk modulus K_M in series with this steady-state viscous element. For $n = 1$, the viscosity η_M is proportional to $D^{-1} \exp[(Q+PV)/RT]$, with the exact form depending on what stress component and strain-rate component are used for σ and $\dot{\varepsilon}_S$ and how the flow law is expressed in three dimensions. Most mantle convection, glacial isostatic adjustment, and SEC models assume $n = 1$, although some include strong temperature dependence and/or spatial variation. This viscosity is a simplified representation of a more complex system that may actually exhibit nonlinearity[4]. Its correspondence with the effective viscosity (a scaled ratio of stress to strain rate) of nonlinear flow cannot be quantified if the stress changes rapidly with time as in postseismic deformation.

A widely used parameterization of the transient creep is the Kelvin (or Kelvin–Voigt) solid, which can be envisioned as an elastic element of shear modulus μ_K in parallel with a viscous element of viscosity η_K. If the transient creep is considered, the simplest model to depict the viscoelastic rock deformation is the bi-viscous Burgers rheology[24], that is, a Kelvin solid in series with a Newtonian Maxwell fluid (see Box 1 Fig. 2). The spatial variation and stress-dependence of η_K are poorly known, although the viscosity ratio $\beta = \eta_M/\eta_K$ is sometimes assumed to be a constant. More complex creep behaviour can be described by including additional Kelvin and/or Maxwell elements. There is a recent attempt to modify the Burgers rheology to include non-Newtonian steady-state creep, but based on an assumption that a stress-independent β can still be defined[34].

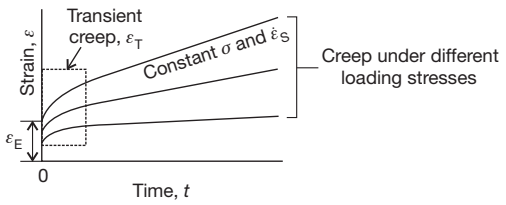

Box 1 Fig. 1 | Strain evolution of a rock specimen under constant stress.

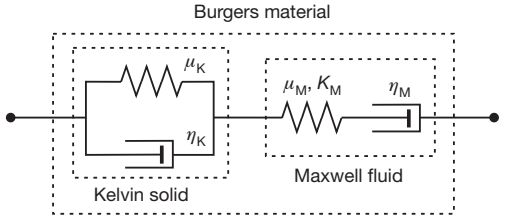

Box 1 Fig. 2 | Composition of the bi-viscous Burgers rheology.

behaviour that is appropriate for long-term processes such as mountain building and mantle convection. The viscous component of Maxwell viscoelasticity corresponds to the steady-state creep. The Maxwell rheology is found to be adequate in modelling century- to millennium-scale glacial isostatic adjustment[24,25] and decadal-scale SEC deformation in Chile[14,17,26] or Alaska[12,13].

The widely used elastic model and a steady-state mantle wedge viscosity of about 10^{19} Pa s in most Maxwell SEC models[8] cannot be reconciled. What may support the elastic model is the enduring notion since 1935 (ref. 25) that upper-mantle viscosity is about 10^{21} Pa s, a value that would render a Maxwell mantle mostly elastic over an SEC of a few centuries. The upper-mantle viscosity structure has been much refined, but a global average of 10^{20}–10^{21} Pa s is still valid[27]. However, there is mounting evidence for lower viscosity at subduction zones, including laboratory measurements of relevant rocks[28], inference of small-scale convection in the backarc based on heat flow observations[29], constraints from topography and geoid anomalies[30], glacial isostatic adjustment analyses[31], as well as the inferences from postseismic deformation[8]. The steady-state viscosity used to explain satellite gravity observations following the 2004 Sumatra earthquake is 10^{18}–10^{19} Pa s (refs 32 and 33).

Continuous GPS monitoring suggests that immediate postseismic deformation and its change with time are much faster than the longer-term behaviour. From rock physics and experiments, it is logical to infer that the rapid short-term deformation reflects not only afterslip but also transient rock creep[34,35]. In recent postseismic deformation models for Sumatra[20,32,33] and the general SEC model in this review (Fig. 1c), a bi-viscous Burgers rheology is employed. The viscoelastic relaxation of the earthquake-induced stress thus has two timescales, a shorter one for the transient viscosity and a longer one for the steady-state viscosity (see Box 1).

Afterslip and relocking of the fault

The ubiquitous presence of afterslip is well recognized. A subduction fault is a zone of finite thickness with evolving internal structure[36], and its slip behaviour is affected by numerous factors including the roughness of the subducting seafloor[37] and amount of trench sediments[38]. But to the first order it is regarded as a frictional contact. Afterslip is thus understood to be the velocity-strengthening behaviour of the fault areas around the rupture zone[39,40]. Deeper than about 70–80 km, where the subduction interface is better described as a zone of localized viscous shear[41], the distinction between afterslip (a fault process) and viscoelastic relaxation (a mantle process) becomes increasingly obscure.

A range of slip behaviour from stable sliding to unstable stick–slip can be explained using a rate-and-state friction law[39,42], but the application of the friction theory to realistic fault geometry and Earth rheology is still in its infancy. In most viscoelastic SEC models it is necessary to prescribe fault motion. The most common way of incorporating fault locking is to assign a backslip rate along the locked zone[43], assuming that steady subduction and its possible consequence in causing permanent surface deformation have been subtracted.

The characteristic timescale of afterslip, T_A, appears to be a few months to a few years[44]. In some cases, if the Earth is assumed to be purely elastic, long-lasting afterslip is used to explain prolonged postseismic deformation[45]. Conversely, there are also cases in which short-term postseismic deformation is explained using viscoelastic relaxation without resorting to afterslip[20,46]. The truth lies in between, and determining T_A and the importance of afterslip relative to viscoelastic relaxation in controlling short-term post-seismic deformation remains a challenge.

In the three primary processes following an earthquake (Fig. 2), fault locking has the longest timescale (T_L), which is simply the length of the interseismic period. Over the past two decades, it has become a common mistake to equate 'interseismic' (a time concept) with 'elastic deformation' (a physical process). Even in recent three-dimensional viscoelastic models, the effect of fault locking is often simulated using an elastic Earth[12–14]. Although the relaxation of the earthquake-induced stress is listed as one primary process in Fig. 2, it cannot be overemphasized that

the other two primary processes also involve their own viscoelastic relaxation[6,26,43]. The stress built up by fault locking is partially relaxed at the same time, regardless of how long after the earthquake and whether the deformation pattern is still changing with time. Given the same locked zone and at a very long time after an earthquake, elastic shortening of the upper plate occurs in a broader zone if the mantle is undergoing viscoelastic relaxation but in a narrower zone if the mantle is purely elastic. For this reason, the maximum depth of locking is usually over-predicted if the viscous effect is not or insufficiently accounted for[15], such as in all the locking models for northeastern Japan published before the Tohoku earthquake[47].

Piecing together an earthquake cycle

Using a numerical SEC model, we demonstrate that the drastically different deformation patterns at the three margins shown in Fig. 3 simply reflect different stages of a common evolution process. Although a site-specific three-dimensional model is needed to describe the structure and kinematics of each margin, the same rheological parameters are used for all the margins. In effect, there is only one physical model. The three margins differ from one another in many aspects, such as the age of the subducting plate and convergence rate. That a similar viscosity structure can be used to explain their first-order SEC is consistent with the observation that the arc–backarc regions of most subduction zones share a similar thermal state[29,41].

This model is an improvement over previously published viscoelastic models for these margins mentioned herein. For example, the use of the finite-element method allows the incorporation of realistic fault geometry and rupture distribution for Sumatra, and both afterslip and transient rheology are included for all the three margins. Because the transient rheology still has a small influence even a few decades after the earthquake, the steady-state viscosity required to explain the Chile observations is slightly lower than in previous models[17,26]. Other important model features (Fig. 1c) include the spherical Earth geometry, which affects far-field deformation, and the presence of an elastic slab, which strongly controls the flow pattern of the mantle material and hence its relaxation process. A continuous distribution of afterslip is assigned that complements coseismic slip in the strike direction, tapers in the updip and downdip directions, and decays with time. Technical details of the modelling and the method of prescribing afterslip by trial-and-error are explained in ref. 48.

The relaxation time of a uniform Maxwell body of viscosity η_M and rigidity μ_M is $\tau_M = \eta_M/\mu_M$. For the subduction zone system, a mixture of elastic and viscoelastic materials, we define an empirical steady-state system-relaxation time $T_M = (M_o/M_o^o)\tau_M$, where τ_M is the Maxwell time of the isoviscous mantle wedge, M_o is the seismic moment (the product of rigidity, rupture area, and mean slip) of the earthquake that causes the stress perturbation, and M_o^o is a reference moment. The relationship between M_o and M_w (ref. 49) gives $\log(M_o/M_o^o) = 1.5(M_w - M_w^o)$, where M_w^o corresponds to M_o^o. The role of rupture length, which two-dimensional models fail to account for, is reflected in this scaling factor. Similarly, we define an empirical transient system-relaxation time $T_K = (M_o/M_o^o)\tau_K$, where $\tau_K = \eta_K/\mu_K$ is the Kelvin time for the mantle wedge of transient viscosity η_K and rigidity μ_K. We assume $\mu_M = \mu_K = 64$ GPa, $\eta_M = 10^{19}$ Pa s, and $\eta_K = 5 \times 10^{17}$ Pa s. These viscosity values are similar to those used in previous Sumatra models[20,32,33] that employed an analytical solution in a spherical viscoelastic Earth. For $M_w^o = 8.4$, these parameters give $T_K \approx 4$ yr and $T_M \approx 80$ yr for an earthquake of $M_w = 9.2$. We also assume that the mantle wedge is less viscous than the oceanic mantle by a factor of ten because of the presence of fluids from the dehydrating slab[8,28,30]. The higher-viscosity 10^{20} Pa s for the oceanic mantle is similar to the global mantle average[27]. To focus on the first-order physics, we have intentionally ignored the spatial variations of the viscosities through their dependence on temperature T, pressure P and fluid contents. Uncertainties and approximations in the viscosity structure are responsible for the arbitrariness in the choice of M_o^o in scaling T_M and T_K with earthquake size.

In explaining geodetic observations, there is a trade-off between T_A, T_K and T_M, reflecting uncertainties in the parameter values. η_M is better constrained by the observed opposing motion in Chile but can vary by a factor of two in the Sumatra and Cascadia models without significantly affecting the fit to the GPS data. Up to three years of GPS data from Sumatra require both afterslip and transient mantle rheology and help to determine T_A and η_K (ref. 48). New observations following more recent great earthquakes such as the $M_w = 8.8$ Maule event in 2010, just north of the 1960 Chile rupture (Fig. 3b), and the Tohoku event in 2011 will surely provide better constraints in the near future.

The three primary processes (Fig. 2) begin immediately after the earthquake, but they take turns to play dominant roles. At times comparable to T_A and T_K, the effect of Maxwell relaxation and fault locking are overshadowed by that of the afterslip and transient (Kelvin) rheology. The dominance of the afterslip and transient rheology cause rapid seaward motion at Sumatra (Fig. 3a). The Sumatra results also explain the present wholesale seaward motion in northeast Japan following the Tohoku earthquake. At times comparable to T_M, the effects of both Maxwell relaxation and locking become dominant, but the two processes give rise to contrasting surface motions (Fig. 2). For Chile (Fig. 3b), sites far away from the trench are still moving seaward because of Maxwell relaxation, but coastal sites are already moving landward because of fault locking. The Chile results also explain the opposing motion currently seen in Alaska[12,13]. Eventually, at times much longer than T_M, the earthquake-induced stresses will be sufficiently relaxed, and the effect of fault locking dominates the entire upper plate. This is the situation currently seen at Cascadia (Fig. 3c). The Cascadia results also explain the wholesale landward motion observed before the Tohoku earthquake[47].

Scaling with earthquake size

The reason that T_K and T_M scale with the seismic moment is that the timescale of relaxation depends on the initial stress perturbation. For example, longer ruptures tend to excite longer-wavelength relaxation modes, which are generally associated with correspondingly longer relaxation times owing to the space-dispersive nature of the relaxation process[50]. Therefore, after a smaller earthquake the effect of fault locking becomes dominant more quickly, such that the Sumatra-type seaward motion and the Chile-type opposing motion are short-lived or even absent[26]. Failure to recognize this scaling was a fatal limitation of earlier two-dimensional models and caused doubts about the necessity of viscoelasticity. Here we illustrate the general role of earthquake size (Fig. 4), using idealized models with the same rheology as discussed above.

These models show how the surface of the upper plate progressively reverses its sense of motion from seaward to landward as the effect of fault locking becomes more dominant. The Extra-large model ($M_w \approx 9.2$), despite its simplicity, is consistent with predictions using models for the three giant events shown in Fig. 3 and current deformation in Alaska and northeastern Japan. It indicates that opposing motion will continue at Chile and Alaska for another few decades and will prevail at Sumatra and northeast Japan within a decade or two. For the Large model ($M_w \approx 8.8$), complete reversal from seaward to landward motion will take a decade or two. We predict this will happen in the area of the $M_w = 8.8$ Maule event of 2010, where wholesale landward motion was observed before the earthquake (northernmost part of Fig. 3b) but wholesale seaward motion is taking place at present[51]. Published examples for the quick reversal illustrated by the Medium model ($M_w \approx 8.4$) include two $M_w \approx 8$–8.1 earthquakes in 1995 in Antofagasta, northern Chile[52] and Colima-Jalisco, Mexico[11]. Some of the GPS sites in the region of the $M_w = 8.3$ Kuril event in 2006 (ref. 46) have now reversed their motion. At the time of the $M_w = 8.4$ Arequipa, Peru, earthquake of 2001 (ref. 40), there was only one continuous GPS station (AREQ) in the affected area, some 200 km from the trench, and it reversed its motion about 6 to 7 years after the earthquake. The exact timing of the reversal depends also on the plate convergence rate, the amount of afterslip, and structural/geometrical details, and therefore may differ from these idealized models. The afterslip behaviour may vary from

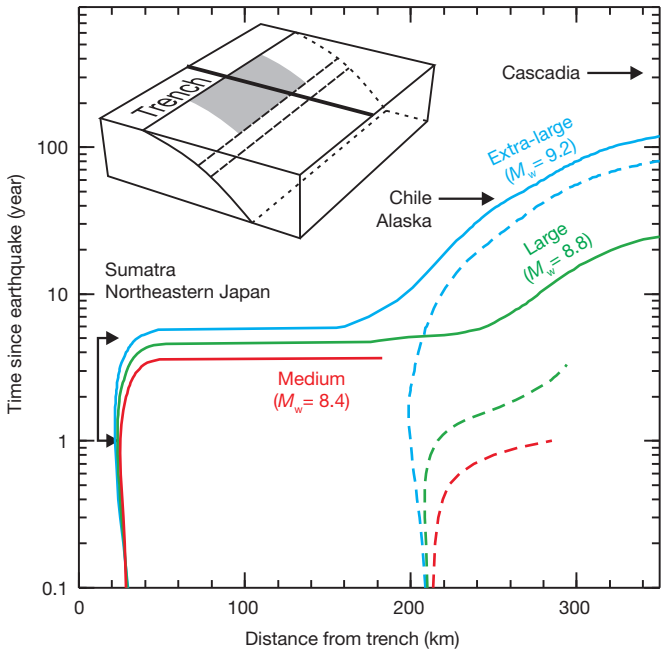

Figure 4 | Evolution of seaward-landward motion transition for different earthquake sizes. For each model, areas to the left of the curve move landward, and those to the right move seaward. The inset shows the model geometry and the line of symmetry (thick line) along which results are shown. Solid and dashed colour lines are results with and without afterslip, respectively. Within each trio, the models differ in rupture length, coseismic slip (assumed to scale with rupture length), and hence earthquake magnitude. The coseismic slip tapers both downdip and updip. The ensuing interseismic locking and its downdip transition (dashed lines) extend to the entire strike length, regardless of the rupture length. Except for the simple geometry and a convergence rate of 5 cm yr^{-1}, all parameters are the same as for Fig. 3. The Extra-large model qualitatively applies to today's deformation fields of the five subduction zones as indicated.

event to event depending on such factors as the structure and fluid pressure of the fault zone.

Also important, but not illustrated here, are along-strike variations in the degree of interseismic locking, as often inferred from geodetic measurements[19,53]. Slowly slipping fault segments serve to load neighbouring, locked patches and thus affect the time and size of future rupture. Such inhomogeneous locking affects interseismic deformation pattern, and more so in the near field.

Looking into the future

Understanding the physics of interseismic deformation helps us to assess seismic and tsunami hazards, because it enables us to infer the locking state of the subduction fault. If viscous mantle creep is ignored, all surface deformation has to be explained by the locking and slip of various parts of the fault, leading to an incorrect depiction of the locking state. Fault-locking scenarios based on elastic models, either via forward modelling or inversion, should be reassessed to include the effect of viscoelastic relaxation. This also applies to other tectonic settings.

Although our present knowledge of Earth's viscoelasticity helps us to address the first-order physics of SEC, there are critical needs for better laboratory and field constraints on the transient rheology and a better understanding of the role of nonlinear rheology. The importance of better characterization and understanding of afterslip is illustrated in Fig. 4 by the large difference in short-term postseismic deformation with and without assuming afterslip. Measurements near the rupture zone are particularly useful. In this regard, ongoing or planned seafloor experiments in the rupture area of the 2011 Tohoku earthquake, such as GPS–acoustic surveys, pressure monitoring, and borehole strain measurements, promise breakthrough discoveries in the next few years. Future seafloor geodesy can also fill the knowledge gap of SEC deformation seaward of the trench and yield critical constraints on the rheology of oceanic mantle.

The SEC deformation needs to be understood in a broad geodynamic context. It seems that the discovery of episodic slow slip events, sometimes accompanied with low-frequency seismic tremor, will soon lead to much improved understanding of the mechanics of the subduction fault and the SEC[54]. Viscoelasticity gives rise to an asymmetry in SEC, that is, coseismic deformation is confined to be near the rupture zone, but interseismic deformation occurs in a broader region[55]. The intriguing implications of this asymmetry for geodynamics and earthquake and tsunami hazards are yet to be explored.

1. Elsasser, W. M. in *The Application of Modern Physics to the Earth and Planetary Interiors* (ed. Runcorn, S. K.) 223–246 (John Wiley, 1969).
2. Bott, M. H. P. & Dean, D. S. Stress diffusion from plate boundaries. *Nature* **243,** 339–341 (1973).
3. Nur, A. & Mavko, G. Postseismic viscoelastic rebound. *Science* **183,** 204–206 (1974).
4. Schubert, G., Turcotte, D. L. & Olsen, P. *Mantle Convection in the Earth and Planets* (Cambridge University Press, 2001).
This book provides a comprehensive review of mantle rheology, Earth structure, theory of mantle convection, and fundamental questions to be addressed by the study of geodynamics.
5. Cohen, S. Numerical models of crustal deformation in seismic zones. *Adv. Geophys.* **41,** 133–231 (1999).
6. Thatcher, W. & Rundle, J. B. A viscoelastic coupling model for the cyclic deformation due to periodically repeated earthquakes at subduction zones. *J. Geophys. Res.* **89,** 7631–7640 (1984).
This paper explains century-long levelling data from southwest Japan in terms of earthquake-cycle deformation and discusses short-term versus long-term postseismic deformation.
7. Matsu'ura, M. & Sato, T. A dislocation model for the earthquake cycle at convergent plate boundaries. *Geophys. J. Int.* **96,** 23–32 (1989).
8. Wang, K. in *The Seismogenic Zone of Subduction Thrust Faults* (eds Dixon, T. H. & Moore, J. C.) 540–574 (Columbia University Press, 2007).
9. Savage, J. C. & Thatcher, W. Interseismic deformation at the Nankai Trough, Japan, subduction zone. *J. Geophys. Res.* **97,** 11117–11135 (1992).
10. Wang, K., He, J., Dragert, H. & James, T. S. Three-dimensional viscoelastic interseismic deformation model for the Cascadia subduction zone. *Earth Planets Space* **53,** 295–306 (2001).
11. Márquez Azúa, B., DeMets, C. & Masterlark, T. Strong interseismic coupling, fault afterslip, and viscoelastic flow before and after the Oct. 9, 1995 Jalisco-Colima earthquake: continuous GPS measurements from Colima, Mexico. *Geophys. Res. Lett.* **29,** 1281 (2002).
12. Suito, H. & Freymueller, J. T. A viscoelastic and afterslip postseismic deformation model for the 1964 Alaska earthquake. *J. Geophys. Res.* **114,** B11404 (2009).
13. Ali, S. T. & Freed, A. M. Contemporary deformation and stressing rates in Southern Alaska. *Geophys. J. Int.* **183,** 557–571 (2010).
14. Moreno, M. S. *et al.* Heterogeneous plate locking in the South–Central Chile subduction zone: building up the next great earthquake. *Earth Planet. Sci. Lett.* **305,** 413–424 (2011).
15. Wang, K., Wells, R., Mazzotti, S., Hyndman, R. D. & Sagiya, T. A revised dislocation model of interseismic deformation of the Cascadia subduction zone. *J. Geophys. Res.* **108** (B1), 2026 (2003).
16. McCaffrey, R. *et al.* Fault locking, block rotation and crustal deformation in the Pacific Northwest. *Geophys. J. Int.* **169,** 1315–1340 (2007).
17. Wang, K. *et al.* Crustal motion in the zone of the 1960 Chile earthquake: detangling earthquake-cycle deformation and forearc-sliver translation. *Geochem. Geophys. Geosyst.* **8,** Q10010 (2007).
18. Khazaradze, G. *et al.* Prolonged post-seismic deformation of the 1960 great Chile earthquake and implications for mantle rheology. *Geophys. Res. Lett.* **29,** 2050 (2002).
19. Freymueller, J. T. *et al.* in *Active Tectonics and Seismic Potential of Alaska* (eds Freymueller, J. T., Haeussler, P. J., Wesson, R. L. & Ekstrom, G.) Geophys. Monogr. Ser. 179 1–42 (American Geophysical Union, 2008).
20. Pollitz, F., Banerjee, P., Grijalva, K., Nagarajan, B. & Burgmann, R. Effect of 3-D viscoelastic structure on post-seismic relaxation from the 2004 M= 9.2 Sumatra earthquake. *Geophys. J. Int.* **173,** 189–204 (2008).
21. Shearer, P. & Bürgmann, R. Lessons learned from the 2004 Sumatra-Andaman megathrust rupture. *Annu. Rev. Earth Planet. Sci.* **38,** 103–131 (2010).
This review of the study of the 2004 Sumatra earthquake shows how geology, seismology, and space geodesy can be combined to investigate coseismic and postseismic deformation and tsunami processes.
22. Grijalva, K. A., Bürgmann, R. & Banerjee, P. Using postseismic geodetic data to constrain the Sunda downdip transition zone. *Eos (Fall Meet. Suppl.)* **90** (52), abstr. T13E–01 (2009).
23. Weertman, J. & Weertman, J. R. High temperature creep of rock and mantle viscosity. *Annu. Rev. Earth Planet. Sci.* **3,** 293–315 (1975).
24. Peltier, W. R., Wu, P. & Yuen, D. A. in *Anelasticity in the Earth* (eds Stacey, F. D., Paterson, M. S. & Nicolas, A.) Geodynamics Ser. 4 59–77 (American Geophysical Union, 1981).
25. Mitrovica, J. X. Haskell [1935] revisited. *J. Geophys. Res.* **101** (B1), 555–569 (1996).

26. Hu, Y., Wang, K., He, J., Klotz, J. & Khazaradze, G. Three-dimensional viscoelastic finite element model for post-seismic deformation of the great 1960 Chile earthquake. *J. Geophys. Res.* **109,** B12403 (2004).
27. Moucha, R., Forte, A. M., Mitrovica, J. X. & Daradich, A. Lateral variations in mantle rheology: implications for convection related surface observables and inferred viscosity models. *Geophys. J. Int.* **169,** 113–135 (2007).
28. Hirth, G. & Kohlstedt, D. L. in *Inside the Subduction Factory* (ed. Eiler, J.) 83–105 (American Geophysical Union, 2003).
29. Currie, C. A. & Hyndman, R. D. The thermal structure of subduction zone back arcs. *J. Geophys. Res.* **111,** B08404 (2006).
30. Billen, M. I. & Gurnis, M. A low viscosity wedge in subduction zones. *Earth Planet. Sci. Lett.* **193,** 227–236 (2001).
31. James, T. S., Clague, J. J., Wang, K. & Hutchinson, I. I. Postglacial rebound at the northern Cascadia subduction zone. *Quat. Sci. Rev.* **19,** 1527–1541 (2000).
32. Panet, I. *et al.* Upper mantle rheology from GRACE and GPS postseismic deformation after the 2004 Sumatra–Andaman earthquake. *Geochem. Geophys. Geosyst.* **11,** Q06008 (2010).
33. Han, S.-C., Sauber, J., Luthcke, S. B., Ji, C. & Pollitz, F. F. Implications of postseismic gravity change following the great 2004 Sumatra-Andaman earthquake from the regional harmonic analysis of GRACE intersatellite tracking data. *J. Geophys. Res.* **113,** B11413 (2008).
34. Freed, A. M., Hirth, G. & Behn, M. D. Using short-term postseismic displacements to infer the ambient deformation conditions for the upper mantle. *J. Geophys. Res.* **117,** B01409 (2012).
35. Pollitz, F. F. Transient rheology of the uppermost mantle beneath the Mojave Desert, California. *Earth Planet. Sci. Lett.* **215,** 89–104 (2003).
36. Bachmann, R. *et al.* Exposed plate interface in the European Alps reveals fabric styles and gradients related to an ancient seismogenic coupling zone. *J. Geophys. Res.* **114,** B05402 (2009).
37. Wang, K. & Bilek, S. L. Do subducting seamounts generate or stop large earthquakes? *Geology* **39,** 819–822 (2011).
38. Scholl, D. W., Kirby, S. H. & von Huene, R. Exploring a link between great and giant megathrust earthquakes and relative thickness of sediment and eroded debris in the subduction channel to roughness of subducted relief. *AGU Fall Meet.* abstr. T14B–01 (2011).
39. Scholz, C. H. Earthquakes and friction laws. *Nature* **391,** 37–42 (1998).
This paper reviews fundamentals of rate- and state-dependent friction and applications to earthquakes and aseismic fault slip.
40. Perfettini, H., Avouac, J.-P. & Ruegg, J.-C. Geodetic displacements and aftershocks following the 2001 $M_w = 8.4$ Peru earthquake: implications for the mechanics of the earthquake cycle along subduction zones. *J. Geophys. Res.* **110,** B09404 (2005).
41. Wada, I. & Wang, K. Common depth of slab-mantle decoupling: reconciling diversity and uniformity of subduction zones. *Geochem. Geophys. Geosyst.* **10,** Q10009 (2009).
42. Hetland, E. A. & Simons, M. Post-seismic and interseismic fault creep. II: Transient creep and interseismic stress shadows on megathrusts. *Geophys. J. Int.* **181,** 99–112 (2010).
43. Savage, J. C. A dislocation model of strain accumulation and release at subduction zones. *J. Geophys. Res.* **88,** 4984–4996 (1983).
44. Pritchard, M. E. & Simons, M. An aseismic slip pulse in northern Chile and along-strike variations in seismogenic behaviour. *J. Geophys. Res.* **111,** B08405 (2006).
45. Sawai, Y. *et al.* Transient uplift after a 17th-century earthquake along the Kuril subduction zone. *Science* **306,** 1918–1920 (2004).
46. Kogan, M. G. *et al.* The mechanism of postseismic deformation triggered by the 2006–2007 great Kuril earthquakes. *Geophys. Res. Lett.* **38,** L06304 (2011).
47. Simons, M. *et al.* The 2011 magnitude 9.0 Tohoku-oki earthquake: mosaicking the megathrust from seconds to centuries. *Science* **332,** 1421–1425 (2011).
48. Hu, Y., &. Wang, K. Spherical-Earth finite element model of short-term postseismic deformation following the 2004 Sumatra earthquake. *J. Geophys. Res.*. (in the press).
49. Hanks, T. C. & Kanamori, H. A moment magnitude scale. *J. Geophys. Res.* **84,** 2348–2350 (1979).
50. Segall, P. *Earthquake and Volcano Deformation* (Princeton University Press, 2010).
51. Brooks, B. A. *et al.* Andean backarc deformation and the plate boundary earthquake cycle. *AGU Fall Meet.* abstr. S14A–08 (2011).
52. Khazaradze, G. & Klotz, J. Short and long-term effects of GPS measured crustal deformation rates along the south central Andes. *J. Geophys. Res.* **108** (B6), 2289 (2003).
53. Wallace, L. M. & Beavan, J. Diverse slow slip behavior at the Hikurangi ubduction margin, New Zealand. *J. Geophys. Res.* **115,** B12402 (2010).
54. Peng, Z. & Gomberg, J. An integrated perspective of the continuum between earthquakes and slow slip phenomena. *Nature Geosci.* **3,** 599–607 (2010).
55. Wang, K. Coupling of tectonic loading and earthquake fault slips at subduction zones. *Pure Appl. Geophys.* **145,** 537–559 (1995).
56. Chlieh, M. *et al.* Coseismic slip and afterslip of the great M_w 9.15 Sumatra-Andaman earthquake of 2004. *Bull. Seismol. Soc. Am.* **97** (1A), S152–S173 (2007).
57. Bürgmann, R. & Dresen, G. Rheology of the lower crust and upper mantle: evidence from rock mechanics, geodesy and field observations. *Annu. Rev. Earth Planet. Sci.* **36,** 531–567 (2008).

Acknowledgements M. Kogan and M. Chlieh provided unpublished information on GPS station reversal after the 2006 Kuril and 2001 Peru earthquakes, respectively. This is Geological Survey of Canada contribution 20110422.

Author Contributions K.W. designed the study and prepared the manuscript. Y.H. did the numerical modelling. J.H. wrote the modelling code and contributed to the modelling.

Author Information Reprints and permissions information is available at www.nature.com/reprints. The authors declare no competing financial interests. Readers are welcome to comment on the online version of this article at www.nature.com/nature. Correspondence should be addressed to K.W. (kwang@nrcan.gc.ca).